energies

MDPI

Article

Effects of Kaolin Addition on Mechanical Properties for Cemented Coal Gangue-Fly Ash Backfill under Uniaxial Loading

Faxin Li [1], Dawei Yin [1,*], Chun Zhu [2], Feng Wang [1], Ning Jiang [1] and Zhen Zhang [1]

[1] State Key Laboratory of Mine Disaster Prevention and Control, Shandong University of Science and Technology, Qianwangang Road 579, Qingdao 266590, China; lfxsdkjdx@163.com (F.L.); wangfeng@sdust.edu.cn (F.W.); jiangning@sdust.edu.cn (N.J.); 13573247170@163.com (Z.Z.)
[2] School of Earth Sciences and Engineering, Hohai University, Xikang Road 1, Nanjing 210098, China; zhu.chun@hhu.edu.cn
* Correspondence: yindawei@sdust.edu.cn; Tel.: +86-18765927224

Abstract: In this investigation, six groups of cemented coal gangue-fly ash backfill (CGFB) samples with varying amounts of kaolin (0, 10, 20, 30, 40, and 50%) instead of cement are prepared, and their mechanical properties are analyzed using uniaxial compression, acoustic emission, scanning electron microscopy, X-ray diffraction, and Fourier transform infrared spectroscopy. The uniaxial compressive strength, peak strain, and elastic modulus of CGFB samples decreased with the kaolin content. The average uniaxial compressive strength, elastic modulus, and peak strain of CGFB samples with 10% amount of kaolin are close to that of CGFB samples with no kaolin. The contribution of kaolin hydration to the strength of CGFB sample is lower than that of cement hydration, and the hydration products such as ettringite and calcium-silicate-hydrate gel decrease, thereby reducing strength, which mainly plays a role in filling pores. The contents of kaolin affect the failure characteristics of CGFB samples, which show tensile failure accompanied by local shear failure, and the failure degree increases with the kaolin content. The porosity of the fracture surface shows a decreasing trend as a whole. When the amount of kaolin instead of cement is 10%, the mechanical properties of CGFB samples are slightly different from those of CGFB samples without kaolin, and CGFB can meet the demand of filling strength. The research results provide a theoretical basis for the application of kaolin admixture in fill mining.

Keywords: kaolin; cemented coal gangue-fly ash backfill sample; mechanical properties; macroscopic failure; microstructure

Citation: Li, F.; Yin, D.; Zhu, C.; Wang, F.; Jiang, N.; Zhang, Z. Effects of Kaolin Addition on Mechanical Properties for Cemented Coal Gangue-Fly Ash Backfill under Uniaxial Loading. *Energies* **2021**, *14*, 3693. https://doi.org/10.3390/en14123693

Academic Editor: Sarma V. Pisupati

Received: 14 March 2021
Accepted: 17 June 2021
Published: 21 June 2021

1. Introduction

Mine-filling technology processes waste such as coal gangue and fly ash into slurry, which not only reduces the accumulation of solid waste and pollution in coal mines, but also enables effective control of the deformation of overlying strata and surface subsidence in mining areas [1]. However, the application of this technology in coal mines is limited owing to insufficient availability of backfill materials and high costs [2,3]. Therefore, cheap, efficient, and widely available backfill materials are required for mine-filling in the future.

China is rich in kaolin resources and has suitable conditions for development and utilization of kaolin. Kaolin ($Al_2O_3 \cdot 2SiO_2 \cdot 2H_2O$) is a type of fine and soft clay mineral having a "single net layer" structure [4–7]. At present, scholars in China and abroad are studying the influences of kaolin admixtures on mechanical properties and the microstructure of concrete materials. Due to the low activity of kaolin, Chun et al. [8] stimulated the pozzolanic activity of kaolin using high-temperature calcination and found that adding an appropriate amount of kaolin into concrete can greatly improve its compressive strength. Lingyan et al. [9] found that calcined activated kaolin has the greatest effect on the early

strength of concrete admixtures, which increases with the addition of kaolin. When the amount of kaolin is 10%, the strength of the concrete admixture is the highest [10–13]. Meng et al. [14] found that the early strength of cement can be improved by mixing calcined activated kaolin and slag. However, the kaolin production via calcination is a high-temperature process that is cumbersome, consumes high energy, and is expensive. Hao [15] and Yuanyuan et al. [16] found that kaolin can react with $Ca(OH)_2$ slowly at room temperature to form hydration products of cementitious ability, and the hydration reaction with cement can create an alkaline environment and enhance this process. Wei et al. [17] found that kaolin and other mineral admixtures can improve the early strength of cement mortar in an alkaline environment. Annan et al. [18] confirmed the plate morphology of kaolin. The particle size of kaolin is mainly in the range of 0–5 μm, which can be filled into smaller pores of cement paste and be dispersed more evenly, which is conducive to the complete occurrence of chemical reactions. Mengna et al. [19] found that the reaction of kaolin and $Ca(OH)_2$ can produce flocculent substances and platelike crystals. The addition of slag and fly ash is conducive to the diffusion of crystals and destroys the structure of $Ca(OH)_2$, thus reducing the porosity of the cement mortar and improving the density of the slurry and filler–matrix interface. Das et al. [20] found that kaolin contains more SiO_2 and Al_2O_3 under alkaline conditions, leading to a higher pozzolanic activity. Its internal structure contains more chemical bonds, which can weaken the secondary hydration of $Ca(OH)_2$ in cement mortar.

The abovementioned research results are of great significance for understanding the effect of kaolin addition on the properties of cement-based materials such as concrete and mortar. The cost of backfilling can be reduced if cement can be replaced with kaolin in cemented coal gangue-fly ash backfill (CGFB) samples. Moreover, it can provide a new path for resource utilization of kaolin. Therefore, based on the test methods of the loading system, acoustic emission (AE), digital video camera (DVC), scanning electron microscope (SEM), X-ray diffraction (XRD), and Fourier-transform infrared spectroscopy (FTIR), we studied the effects of kaolin partially replacing cement on the mechanical properties of CGFB samples, and the feasibility of using kaolin as paste admixture was discussed. The results can provide a theoretical basis for application of kaolin admixture in fill mining.

2. Materials and Methods

2.1. Raw Materials

As shown in Figure 1, the CGFB samples used in this test are composed of cement, fly ash, gangue, kaolin, and water. Their main components and contents are listed in Table 1.

Table 1. Main components and contents.

Raw Material	Chemical Composition and Content/%											
	SiO_2	Al_2O_3	CaO	Na_2O	SO_3	K_2O	MgO	TiO_2	MnO	Fe_2O_3	ZnO	BaO
Cement	15.722	12.340	51.643	2.177	3.025	1.203	8.706	1.031	0.190	3.891	0.072	—
Fly ash	37.855	39.724	6.214	1.456	1.221	2.118	3.914	2.479	0.055	4.856	0.107	—
Gangue	39.987	30.177	11.727	1.758	2.886	2.643	3.088	2.531	—	4.928	—	0.276
Kaolin	42.153	47.704	—	—	—	5.063	1.276	2.079	—	1.725	—	—

Here, 32.5 grade ordinary Portland cement (OPC) produced by Shandong Rizhao No. 3 cement plant was used. Grade II fly ash from the Huangdao Power Plant in Qingdao City, Shandong Province, which has a light grey appearance, was used. The gangue (particle size < 25 mm) was obtained from the solid waste produced in roadway excavation, coal mining, and separation in the Shandong Daizhuang coal mine. The kaolin was taken from the water-washed kaolin produced by a material factory in Guangdong Province. The 80-μm-square pore sieve residue is less than 8%, and the 45-μm-square pore sieve residue is less than 25%, which meets the technical requirements of general Portland cement (GB/T 175-2007) [21].

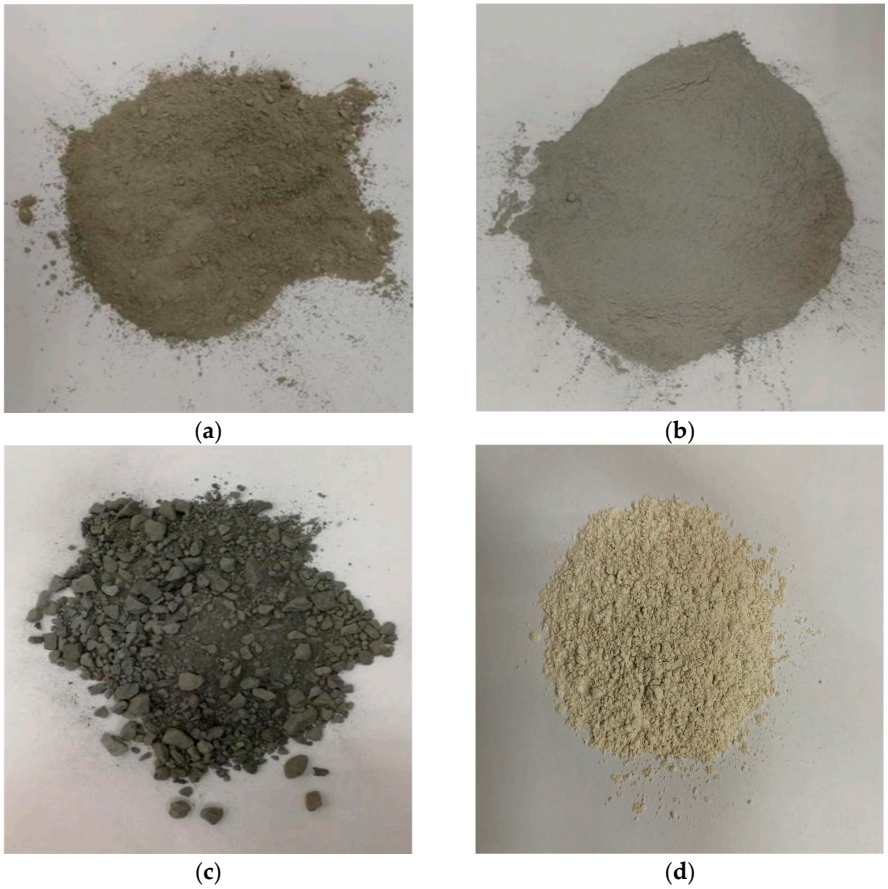

Figure 1. Raw materials. (**a**) Cement; (**b**) Fly ash; (**c**) Gangue; (**d**) Kaolin.

The microscopic morphology of kaolin was analyzed by a scanning electron microscopy (SEM) system. The powder sample was dipped on the conductive adhesive using a wooden stick, and the kaolin surface was plated with gold. The morphology of the sample was observed at 10,000× magnification, as shown in Figure 2a. The layered structure of kaolin particles is evident in the figure, and each block of kaolin particles is composed of many lamellar structures closely superimposed together, with clear edges and corners. The morphology of kaolin particles is irregular and the particle size is different, which is conducive to backfill the internal pores of CGFB samples, increasing its internal occlusal degree and improving its internal structure.

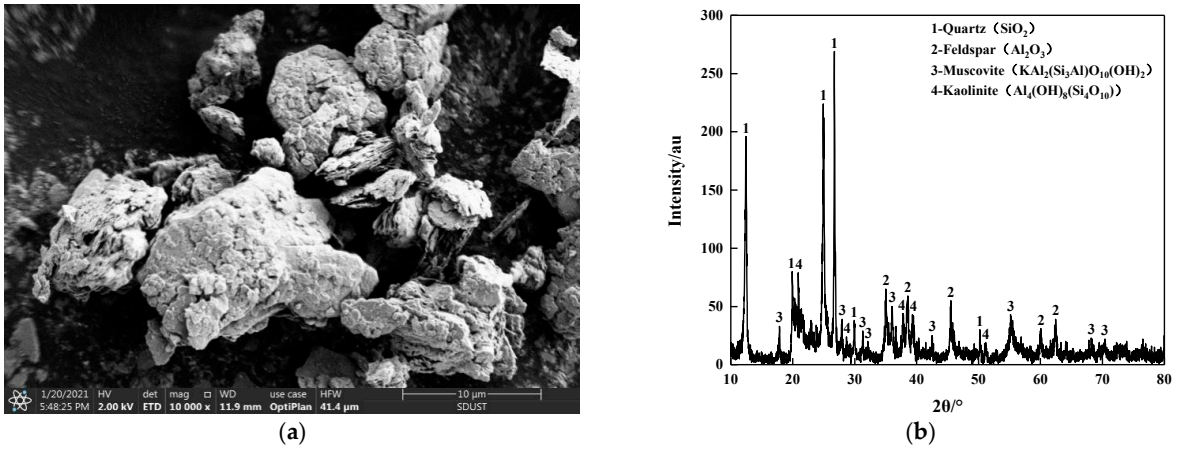

Figure 2. Microstructure analysis of kaolin. (**a**) SEM of kaolin; (**b**) XRD pattern of kaolin.

The crystal phase of the kaolin admixture was analyzed using XRD, as shown in Figure 2b [22]. The XRD patterns show multiple dispersion peaks of quartz, feldspar, muscovite, and kaolinite, among which quartz and feldspar are mainly composed of SiO_2 and Al_2O_3, respectively. The kaolin admixture is rich in active SiO_2 and Al_2O_3, which can replace a part of the cement for pozzolanic reaction and improve the internal bonding of CGFB samples.

2.2. Sample Preparation

In this test, CGFB samples were prepared using cement, fly ash, and gangue in the ratio of 1:4:6; the solid mass fraction was 78%; no additions were added, and the amounts of kaolin replacing cement were 0, 10, 20, 30, 40, and 50%. During the preparation of CGFB samples, an NJ-160 agitator was used for stirring for approximately 8 min. After the slurry was evenly mixed, it was poured into a Φ50 mm $\times$ 100 mm mould. The bubbles in the samples were removed by manual vibration and tamping. CGFB samples were removed from moulds after 24 h and cured for 28 days in a curing box at a temperature of 25 °C and relative humidity of 80%. Before the test, the two ends of the samples were smoothed with a grinding machine: the flatness tolerance of the end face was less than 0.05 mm, and unevenness was less than 0.002 mm [23]. Evident cracks on the surface of the CGFB samples were removed. A total of 18 samples, as shown in Figure 3, were prepared for this test. Based on the amounts of cement replaced with kaolin, they were divided into six groups: A, B, C, D, E, and F, corresponding to cement replacement of 0, 10, 20, 30, 40, and 50% chemically pure (CP), respectively, and each group contained three samples.

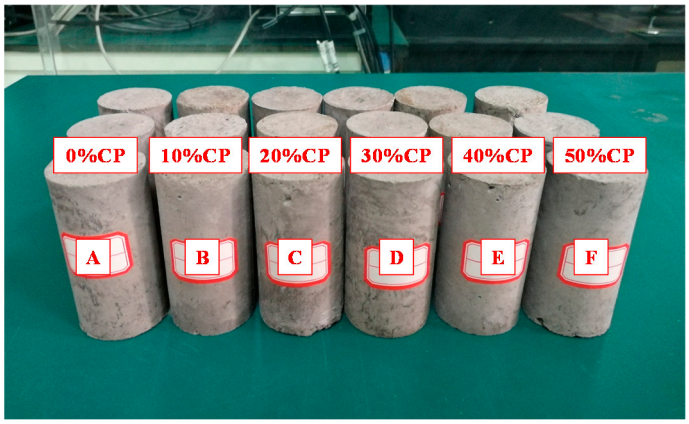

Figure 3. CGFB samples.

2.3. Test Method

The experimental test setup, including the loading, AE, DVC, SEM, XRD, and FTIR systems, is shown in Figure 4. During each test, loading, AE, and DVC systems were synchronized to have the same timestamps to facilitate analysis of the experimental results.

2.3.1. Uniaxial Compression Tests

A Shimadzu AG-X250 electronic universal testing machine was used to conduct the uniaxial compression tests on the CGFB samples. This machine can perform uniaxial compression, tensile, and other mechanical tests using a maximum load of 250 kN [24–27]. When performing uniaxial compression tests, a preload pressure of 0.1 kN was first applied to the test sample, so that the indenter was in close contact with the test piece, and displacement loading control at a loading rate of 0.0005 mm/s was conducted.

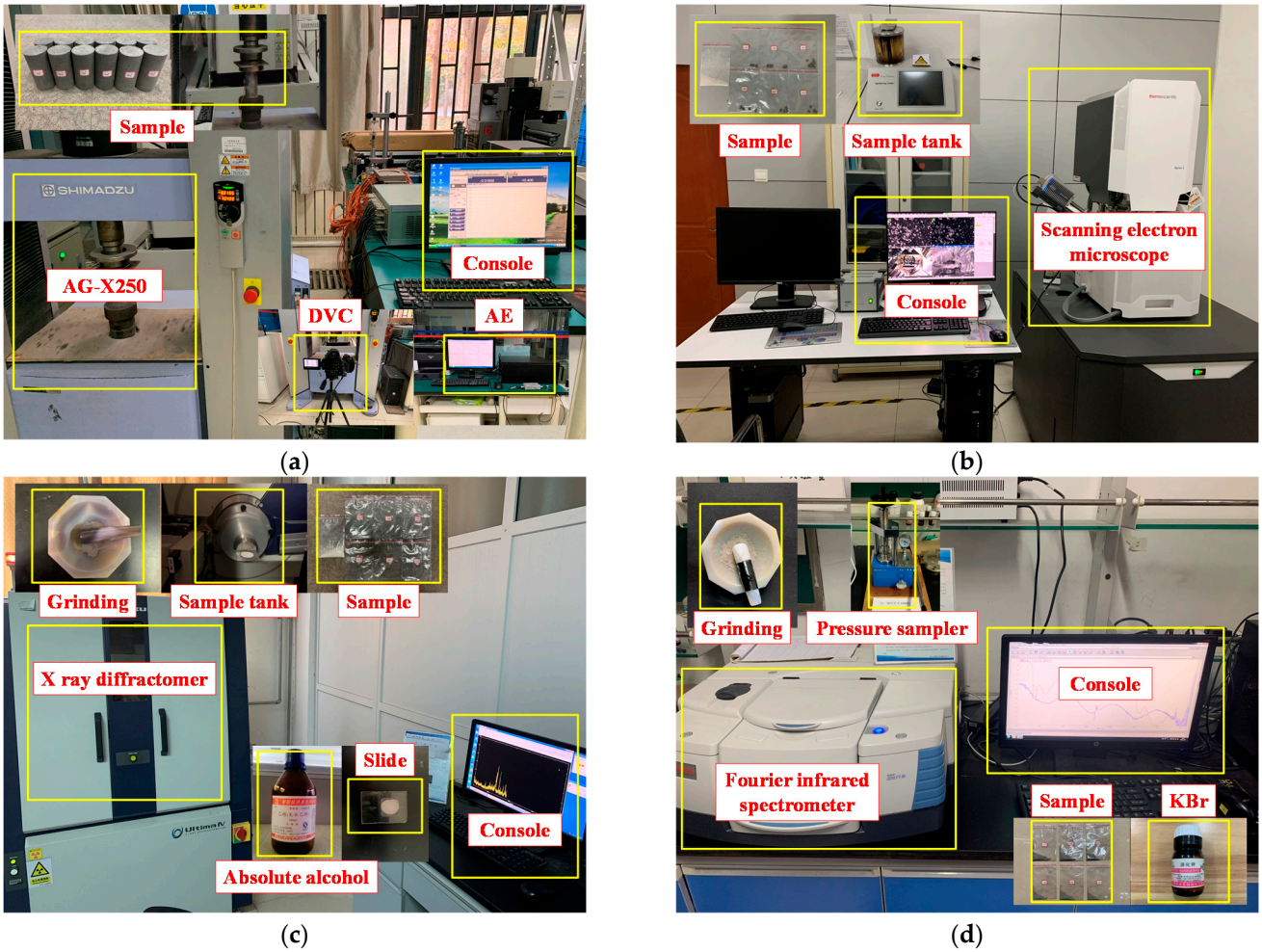

Figure 4. Experimental testing system. (**a**) Uniaxial compression tests; (**b**) SEM experiment; (**c**) XRD experiment; (**d**) FTIR experiment.

2.3.2. Acoustic Emission Experiment

The failure under uniaxial compression was monitored in real-time using the MISTRAS series PCI-2 AE system. An R3α type of AE sensor, a main amplifier of 40 dB, threshold of 45 dB, floating threshold of 6 dB, probe harmonic frequency of 100–600 kHz, and sampling frequency of 10^6 times/s were used [28]. Petroleum jelly (Vaseline) was applied between the sensor and samples for coupling them and reducing the acoustic impedance difference and reflection loss of energy at the interface. This ensured that the sensor received the AE signal with minimal loss. The sensor was fixed with adhesive tape, and the pencil lead fracture method proposed by American Society for Testing and Materials (ASTM) was used to calibrate the AE system for ensuring that the signal amplitude of each sensor was above 90 dB [29]. During the test, a video camera (Sony DVC) was used to record the failure under uniaxial loading.

2.3.3. Scanning Electron Microscopy Experiment

The internal microstructure of the CGFB samples was examined using the Apreo S Hivac high-resolution SEM. The samples were soaked in alcohol and dried. After the surface of the samples was blown clean using an ear-washing ball, they were pasted on the sample table using a conductive adhesive. The internal structure of the samples was observed after the surface was sprayed with gold.

2.3.4. X-ray Diffraction Experiment

The crystal phase of the CGFB samples was analyzed using Rigaku Ultima IV XRD operating at a voltage of 40 kV and an emission current of 40 mA. The dried samples were ground using a mortar and screened using a 200-mesh sieve. During this, fragments with relatively few aggregates (coal gangue) were retained, and large particles such as aggregates (coal gangue) were removed. After the powder sample was tiled on the groove of the glass slide, it was placed into the instrument for testing.

2.3.5. Fourier-Transform Infrared Spectroscopy Experiment

The functional groups on the surface of the CGFB samples were measured using Nicolet iS5 FTIR. When testing samples, the samples were first ground with a mortar and then dried. During this, fragments with relatively few aggregates (coal gangue) were retained, and large particles such as aggregates (coal gangue) were removed. After mixing the samples with pure potassium bromide at a ratio of 1:10, grinding, and pressing, they were placed in the spectrometer and scanned 50 times to obtain the infrared spectrum.

3. Results

3.1. Uniaxial Compression Test Results

The strength of CGFB is an important index for evaluating coal mine safety conditions and backfill effects. In this test, the data are collected synchronously through a computer using a sampling interval of 10 ms. Table 2 shows the uniaxial compressive strength (UCS), peak strain, and elastic modulus of the samples. Figure 5 shows the uniaxial compressive stress–strain curves, while Figure 6 shows comparisons of the UCS, peak strain, and elastic modulus of CGFB samples under different amounts of kaolin.

Table 2. Uniaxial test results of CGFB samples.

Addition	Number	UCS (MPa)	Elastic Modulus (MPa)	Peak Strain (mm/mm)
0%	A-1	0.70	205.47	0.0061
	A-2	0.70	199.66	0.0068
	A-3	0.79	240.75	0.0064
	Average	0.73	215.29	0.0064
10%	B-1	0.58	211.20	0.0043
	B-2	0.80	183.47	0.0054
	B-3	0.67	182.44	0.0060
	Average	0.68	192.37	0.0053
20%	C-1	0.52	169.18	0.0048
	C-2	0.59	166.39	0.0043
	C-3	0.57	141.19	0.0049
	Average	0.56	158.92	0.0047
30%	D-1	0.31	156.33	0.0050
	D-2	0.39	123.17	0.0035
	D-3	0.46	179.88	0.0038
	Average	0.39	153.13	0.0041
40%	E-1	0.45	201.66	0.0025
	E-2	0.46	135.53	0.0045
	E-3	0.43	113.93	0.0037
	Average	0.45	150.37	0.0036
50%	F-1	0.35	72.36	0.0031
	F-2	0.36	90.85	0.0037
	F-3	0.38	61.91	0.0022
	Average	0.36	75.04	0.0030

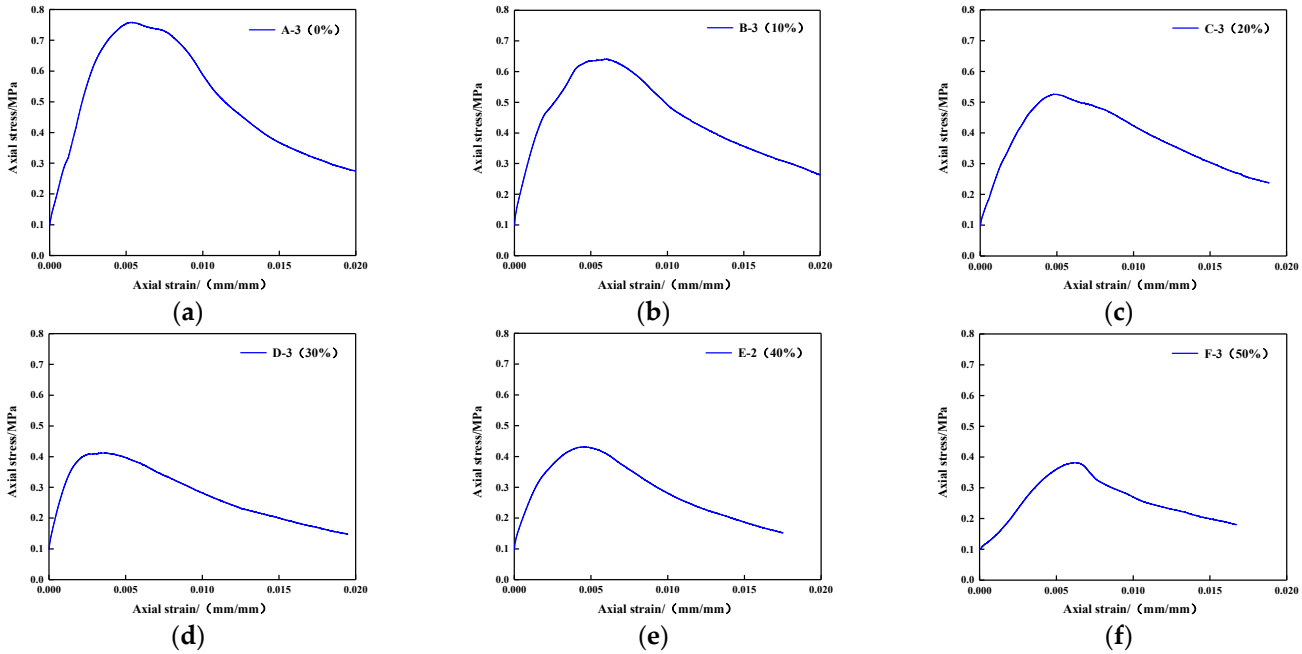

Figure 5. Stress–strain curves of CGFB samples. (**a**) A-3; (**b**) B-3; (**c**) C-3; (**d**) D-3; (**e**) E-2; (**f**) F-3.

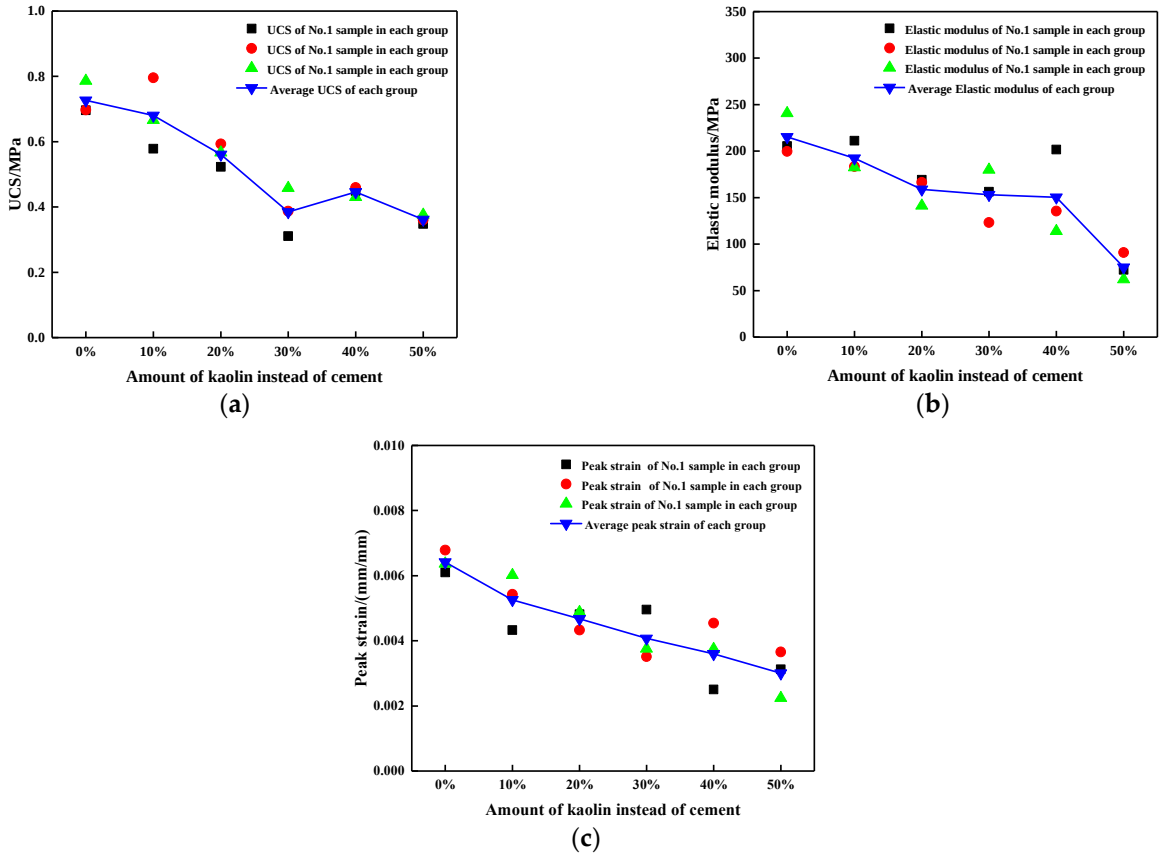

Figure 6. Comparisons of (**a**) UCS, (**b**) elastic modulus, and (**c**) peak strain of CGFB samples under different amounts of kaolin.

As seen from Figure 5, the stress–strain curves of the CGFB samples have the same shape, and they all pass through initial compaction, elastic deformation, plastic yield, and post-peak strain softening stages. However, the values of UCS, peak strain, and elastic

modulus are different, illustrating that the kaolin affects the mechanical properties of CGFB samples. As shown in Figure 6, the UCS, peak strain, and elastic modulus of CGFB samples are affected by the amounts of kaolin replacing cement. CGFB samples with 0% kaolin instead of cement exhibit highest average UCS (0.73 MPa), elastic modulus (215.29 MPa), and peak strain (0.0064), while those with 50% kaolin exhibit lower UCS (0.36 MPa), elastic modulus (75.04 MPa), and peak strain (0.0030). The mechanical properties decrease with the increase of amounts of kaolin instead of cement. The higher the content of kaolin, the better the elasticity, and easier the deformation of CGFB. In addition, the amounts of kaolin instead of cement affect the post-peak strain softening stage of CGFB. The post-peak stress of CGFB decreases with time. The higher the content of kaolin, the smaller the slope of the CGFB curve, and stronger the plastic deformation ability.

In addition, in the Figure 6, it is found that the average values of UCS for CGFB samples decrease integrally with the amounts of kaolin instead of cement. Meanwhile, the values of UCS for the D-3 sample (30% CP) and group E samples (40% CP) show a slight increase. Previous investigations have shown that the strength of the CGFB samples is mainly determined by the cement hydration [30–34]. Generally, the stronger the cement hydration is, the larger the corresponding strength of the CGFB sample is. Normally, the activity of kaolin is lower than that of cement, and the incorporated kaolin only partially replaces cement for hydration reaction. The hydration caused by cement is lower than that of cement. With the increase of kaolin proportion, the amount of cement involved in the hydration reaction decreases. Therefore, the cement hydration effect is weakened, and the UCS of CGFB samples decreases. At the same time, the kaolin, which is not involved in hydration, mainly plays a role in filling the pores of CGFB samples. The average porosities of the failure or fracture surface of CGFB samples decrease with the kaolin content, which are analyzed in Section 3.3. Thus, the integrity of the CGFB samples is enhanced. Based on the above analyses, the strength of the CGFB samples containing kaolin may increase under these two mechanisms of the kaolin on mechanical properties for CGFB samples, but which is lower than that of the CGFB samples without the kaolin.

3.2. Macro Failure Characteristics

Figure 7 shows the macro-failure patterns of CGFB samples, which can be divided into tensile and shear failures, under different amounts of kaolin. The amounts of kaolin indeed affect the failure characteristics of CGFB samples as the failure degree increases with the increase of kaolin instead of cement. When the amount of kaolin is 50%, the highest amount of tensile cracks in CGFB samples is seen. The CGFB samples were gradually fractured along the diagonal direction with the increase of kaolin instead of cement. After the CGFB samples are fractured, the large tensile cracks on their surface increase, and most of them are distributed near the gangue particles. This shows that the decrease of cement content leads to the decrease of internal bonding degree. The ultimate failure characteristics of CGFB samples show tensile failure accompanied by local shear failure.

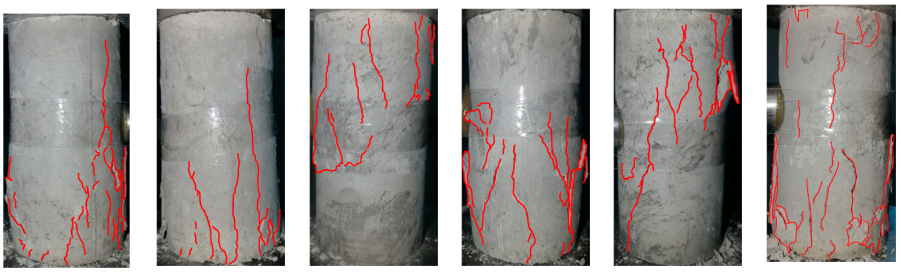

(**a**) (**b**) (**c**) (**d**) (**e**) (**f**)

Figure 7. Failure characteristics of CGFB samples. (**a**) A-1; (**b**) B-2; (**c**) C-2; (**d**) D-3; (**e**) E-3; (**f**) F-3.

A single stress–strain curve cannot reflect the development process, but the failure degree of CGFB samples with different amounts of kaolin addition can be revealed in detail

by analyzing the AE Ra and cumulative Ra value. The different characteristics of tensile failure and shear failure can also be understood in detail. The Ra value of the AE is the ratio of the rise time to amplitude, which is an important index for determining the fracture mode. Shiotani et al. [35] calculated the Ra value of rock under bending and shear tests and concluded that a low Ra value corresponds to a shear crack, while a high Ra value corresponds to a tensile crack.

In Figure 8, the relationship between axial stress and cumulative RA value over time during failure of CGFB samples with different kaolin contents is shown to reveal the failure characteristics. It can be seen that when the CGFB samples without kaolin fail, the initial Ra value is at a low level, and the cumulative Ra value increases slowly, which indicates the occurrence of shear failure. Near peak stress, the Ra value suddenly increases, and the cumulative Ra value increases rapidly. This phenomenon can be understood as the point when the CGFB samples without kaolin start getting compacted under the action of the vertical load, resulting in transverse tensile stress. As alluded to earlier, due to existence of gangue particles and a large number of holes, microcracks, and other defects in CGFB samples, their internal structure is under uneven stress, and the effective bearing area reduces, resulting in shear failure of mutual dislocation initially. With the gradual increase in vertical load, friction between a large number of holes and microcracks also increases, which inhibits mutual dislocation, and CGFB samples attain a stable state. As the load continues increasing and becomes higher than the compressive strength of CGFB samples, a crack begins to develop, and the sample finally fractures.

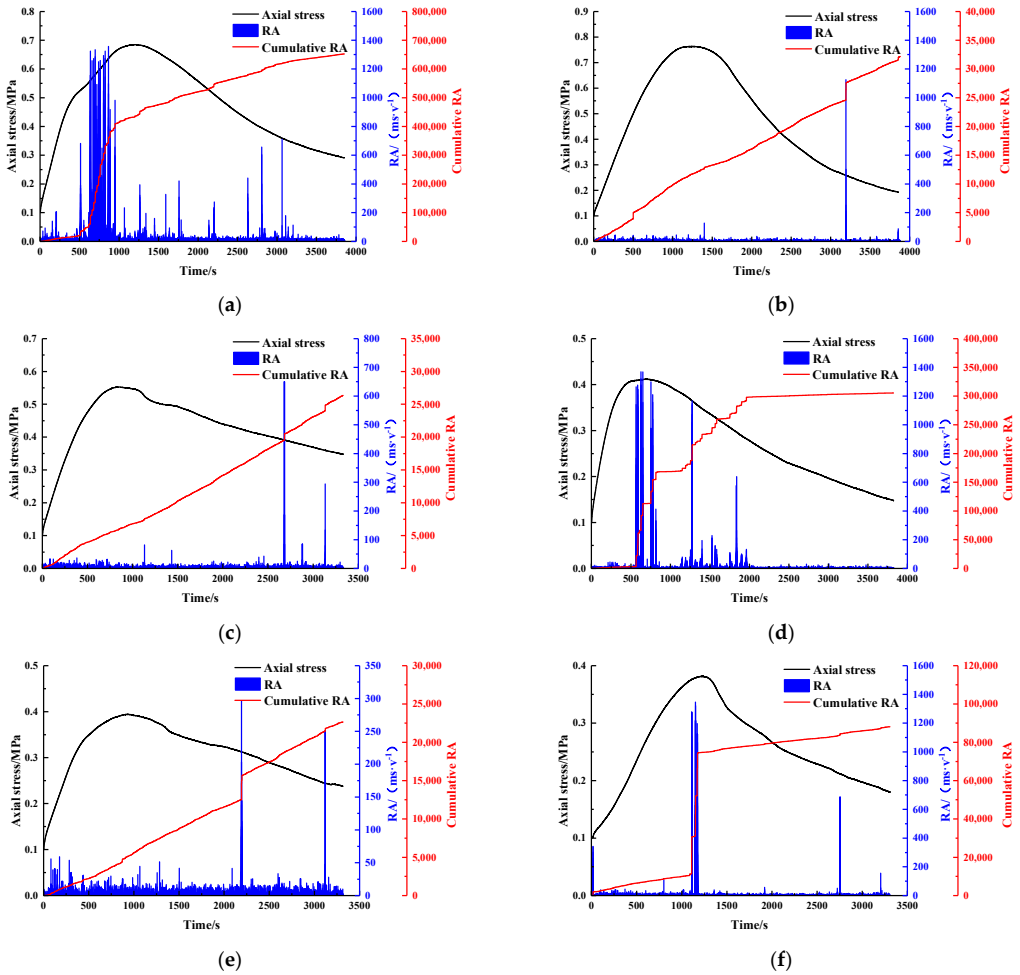

Figure 8. Acoustic emission (AE) characteristics of CGFB samples. (**a**) A-1; (**b**) B-2; (**c**) C-2; (**d**) D-3; (**e**) E-3; (**f**) F-3.

With the increase of the amount of kaolin instead of cement, the fluctuation of the Ra value of CGFB samples increases, and the difference of its cumulative Ra value decreases, which increases the number of tensile cracks in CGFB samples. This shows that a decrease in the cement content leads to a decrease in the degree of internal bonding. During the compression process, a large amount of elastic energy is stored in the gangue particles. With the increase in sample deformation, energy is released near the gangue particles and causes chain failure of the surrounding structure, resulting in tensile failure accompanied by local shear failure of the sample.

3.3. Microstructure Characteristics

The microstructure and morphology of the fracture surface of CGFB samples are analyzed using SEM and are shown in Figure 9. It can be seen that the microstructure and morphology of fracture surfaces of different CGFB samples are different. Because of the disappearance of the coating layer on the surface of CGFB samples, the rate of hydration reaction increases, and a large amount of flocculated calcium-silicate-hydrate (C-S-H) gel forms in the main body. Ettringite (AFt) having a needle-like structure is mostly distributed in pores. These crystals are closely connected, which improves the strength of the sample. When the amount of kaolin is 10%, more hydration products (AFt and C-S-H gel) are observed. The internal structure of the samples is compact, and the number of pores is small. When the amount of kaolin is more than 10%, the number of hydration products decreases, and that of irregular particles increases. At 50% kaolin content, fewer hydration products are observed, but the internal structure is relatively dense, which indicates that kaolin mainly fills the pores in higher quantities.

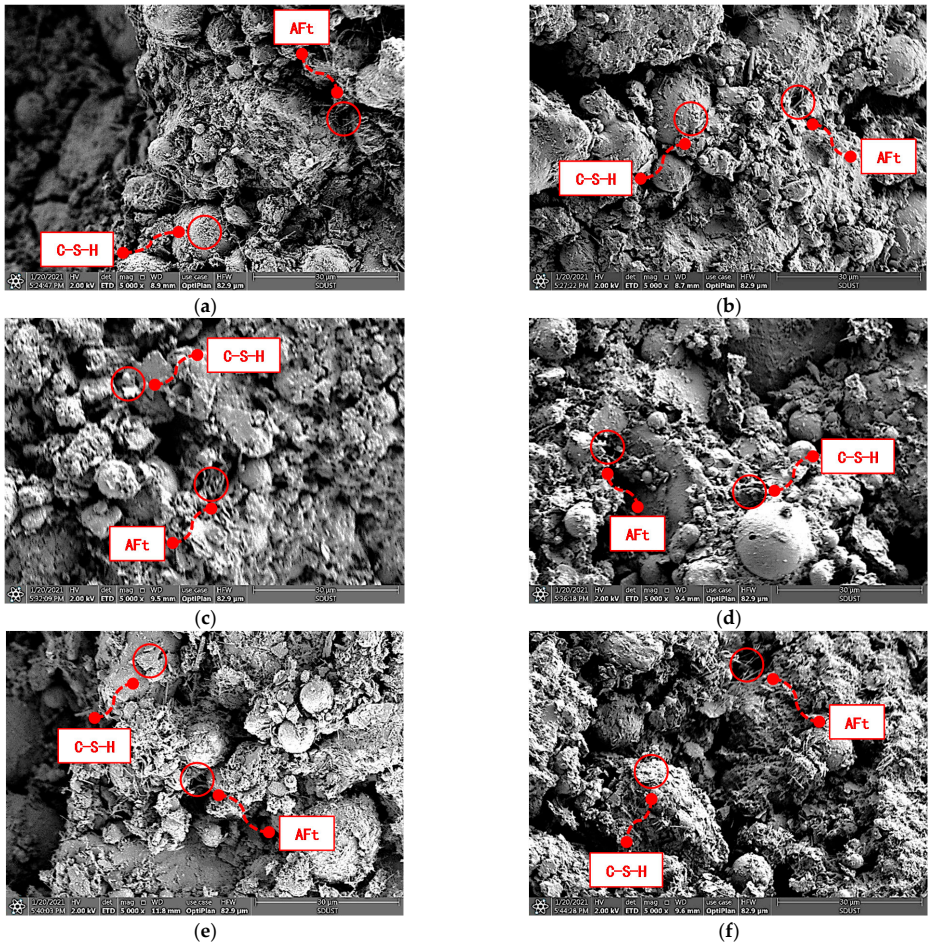

Figure 9. SEM image of fracture surface of CGFB samples. (**a**) 0% CP; (**b**) 10% CP; (**c**) 20% CP; (**d**) 30% CP; (**e**) 40% CP; (**f**) 50% CP.

PCAS is a professional software tool for the identification and quantitative analysis of pore systems and fracture systems [36]. It can automatically identify all types of pores and fractures in images and obtain all geometric and statistical parameters. Concerning pore recognition, it can import various pore images, remove clutter automatically, segment and recognize pores automatically through binarization, output the geometric and statistical parameters, and display the result vector image and rose diagram. It can also display various geometric parameters of all pores in the data table, including the number of pores, area, length, width, directivity, and shape coefficient, and obtain statistical parameters such as region percentage (porosity), average form factor, probability entropy, fractal dimension, and sorting coefficient [37]. In this study, PCAS is used to quantitatively analyze the micropore structure of CGFB samples. The pore map after PCAS processing is shown in Figure 10, where the black zone represents the non-porous area, and the colored zone represents pores where the software automatically recognizes and artificially corrects some recognition errors and defects. For different pores (unconnected pores), the PCAS uses a different color mark, while the same color mark is used for connected pores [38]. All CGFB samples are observed and analyzed in this manner. The minimum diameter of the closed pore in PCAS is 2, and the minimum pore area is 50. The region percentages (porosities) of the samples are listed in Table 3.

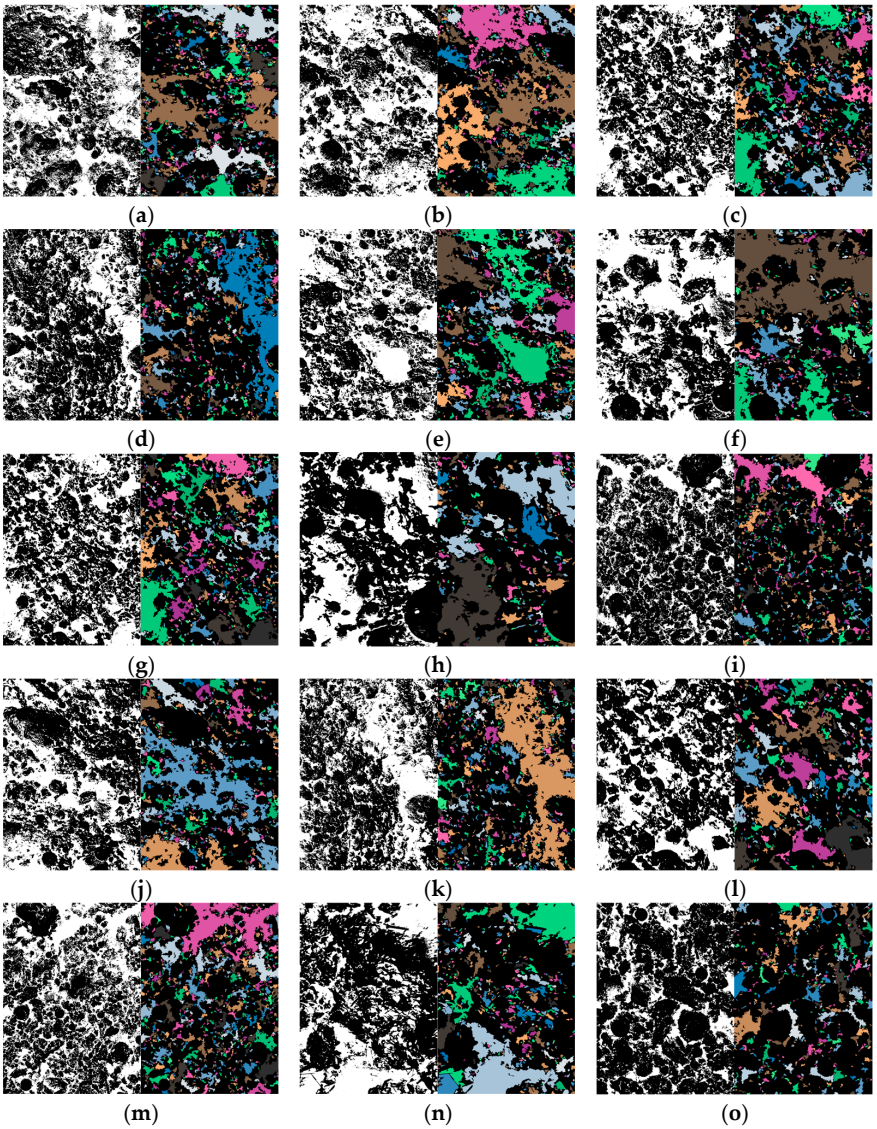

Figure 10. *Cont.*

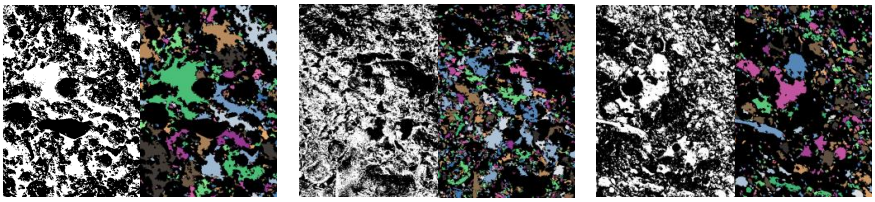

(**p**) (**q**) (**r**)

Figure 10. Binarization of CGFB microscopic pores. (**a**) A-1; (**b**) A-2; (**c**) A-3; (**d**) B-1; (**e**) B-2; (**f**) B-3; (**g**) C-1; (**h**) C-2; (**i**) C-3; (**j**) D-1; (**k**) D-2; (**l**) D-3; (**m**) E-1; (**n**) E-2; (**o**) E-3; (**p**) F-1; (**q**) F-2; (**r**) F-3.

Table 3. Region percentage (porosity) of CGFB samples.

Addition	Number	Region Percentage (Porosity)
0%	A-1	43.26%
	A-2	49.45%
	A-3	41.26%
	Average	44.66%
10%	B-1	33.52%
	B-2	45.21%
	B-3	46.56%
	Average	41.76%
20%	C-1	41.27%
	C-2	39.64%
	C-3	39.94%
	Average	40.28%
30%	D-1	39.08%
	D-2	39.54%
	D-3	38.47%
	Average	39.03%
40%	E-1	37.08%
	E-2	36.04%
	E-3	36.05%
	Average	36.39%
50%	F-1	35.07%
	F-2	34.84%
	F-3	32.77%
	Average	34.23%

Many studies [39–42] have shown that porosity has a significant relationship with UCS. Table 3 shows the porosity of CGFB samples with different amounts of kaolin instead of cement. The average porosity of each group of CGFB is compared with the average UCS, and their relationship under different amounts of kaolin instead of cement is shown in Figure 11.

Generally speaking, when the porosity of CGFB samples decreases, the UCS also decreases. However, in Figure 11, an opposite trend is seen. The reason is that the hydration is the main factor of kaolin affecting the strength of CGFB samples. The activity of kaolin is lower than that of cement, but with the increase of kaolin content, the hydration of cement decreases, so the UCS of CGFB samples decreases. However, kaolin also fills the internal pores of CGFB samples, which improves their integrity and reduces the corresponding porosity. In summary, the porosity of CGFB samples decreases with the increase of kaolin instead of cement, and the UCS gradually decreases.

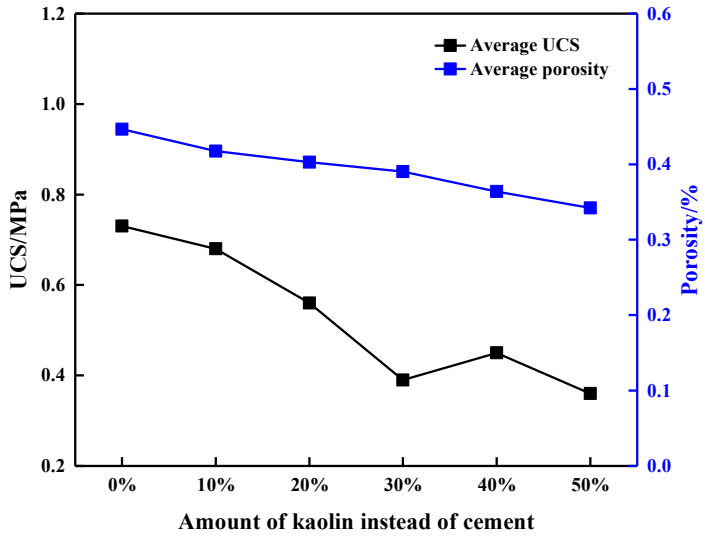

Figure 11. Comparison of the relationship between UCS and porosity of CGFB with different amount of kaolin instead of cement.

4. Discussion

The goal of coal mine filling is to meet the needs of coal mine production safety at the lowest possible cost. Therefore, the selection of appropriate CGFB samples material is related not only to the filling cost but also the safety and stability of the goal. After adding kaolin into CGFB samples, the sample will have effects of morphology, micro-aggregate, and activity of the kaolin admixture. The morphological effects of kaolin addition are mainly reflected in the influence of kaolin particle size, shape, and other factors on the performance of CGFB samples. The micro-aggregate effects are that the particles are relatively fine and can be evenly dispersed in the gangue aggregate and flocculation structure, filling the internal pores, which helps improve the internal uniformity of CGFB samples. Kaolin is rich in active SiO_2 and Al_2O_3. The essence of its pozzolanic activity is that SiO_2 and Al_2O_3 are excited in alkaline environments. The content of soluble active components in kaolin is very low; therefore, the degree of pozzolanic reaction of kaolin is low initially.

To study the influence of different amounts of kaolin content on the hydration products of CGFB samples, phases of CGFB samples cured for 28 days are analyzed via XRD, and the diffraction patterns are shown in Figure 12. Similar diffraction patterns of CGFB samples are seen, but the intensity of the peaks is different from that of the hydrated products, which form $Ca(OH)_2$, C-S-H gel, AFt, etc. When the amount of kaolin is less than 10%, the peak of $Ca(OH)_2$ becomes weaker, the SiO_2 peak becomes stronger, and the C-S-H gel diffraction peak becomes stronger with an increase in the amount of kaolin instead of cement. This indicates that some active substances in kaolin consume $Ca(OH)_2$ to participate in the two hydration reactions. When the amounts of kaolin instead of cement are greater than 10%, the peak value of SiO_2 continues to increase, and the diffraction peaks of $Ca(OH)_2$, AFt, and C-S-H become weak with an increase in the amount of kaolin content. This shows that after a certain point of kaolin addition, reduction in cement content per unit volume will negatively affect the secondary hydration of kaolin.

To further investigate the effects of kaolin on CGFB samples, the chemical structures of the prepared samples are characterized via FTIR spectroscopy. Figure 13 shows the infrared spectrum of CGFB samples, which shows that FTIR spectra of CGFB samples are similar. The broad absorption band at wavenumbers of 2976.99–3592.77 cm^{-1} characterizes the stretching vibration of Al-OH in the [AlO_4] tetrahedron, and the absorption peak of 1588.25 to 1784.38 cm^{-1} represents the bending vibration of H_2O in C-S-H [43]. Absorption peaks at 1349.18–1588.25 cm^{-1} represent the O-C-O asymmetric stretching vibration of carbonate, indicating that the CGFB samples experienced slight carbonization

during the characterization process [44]. Absorption peaks of 936.78–1349.18 cm^{-1} corresponds to the asymmetric stretching vibration of Si-O in tetrahedron [45], while those at 820.31–886.33 cm^{-1} reflects the existence of [Al(Fe)-O], which means that some Al-OH in AFt is replaced by Fe-OH [46].

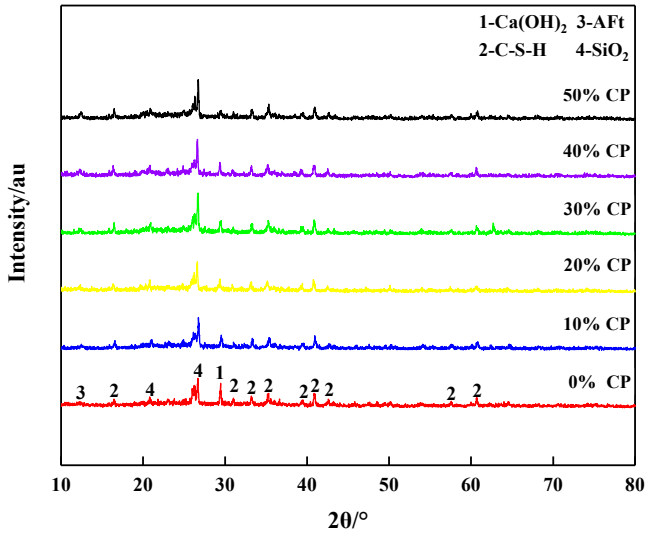

Figure 12. XRD patterns of CGFB samples.

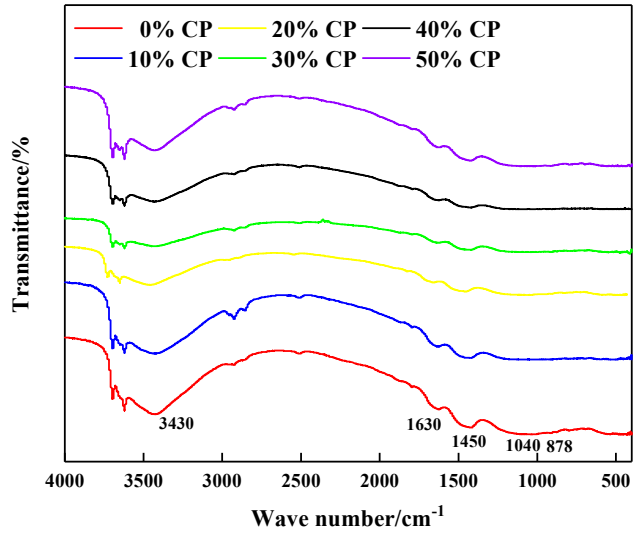

Figure 13. FTIR spectrum of CGFB samples.

Figure 14 gives the pozzolanic reaction of kaolin in the CGFB sample. Pore water rich in Ca^{2+}, AlO_2^-, and SiO_3^{2-} first infiltrate CGFB, and the cement particles in CGFB samples hydrate to form $Ca(OH)_2$ and other products in the liquid phase. The hydration reaction of cement is as follows:

$$C_3S + nH \rightarrow C\text{-}S\text{-}H + (3\text{-}x)\ CH \quad (1)$$

$$C_2S + mH \rightarrow C\text{-}S\text{-}H + (2\text{-}x)\ CH \quad (2)$$

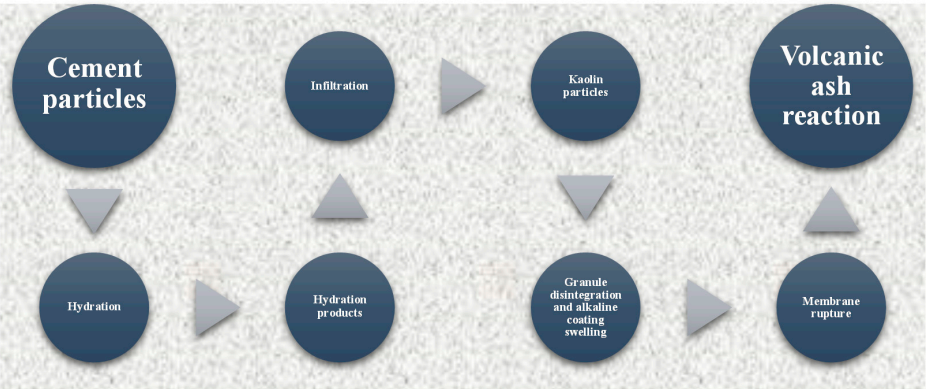

Figure 14. Pozzolanic reaction process of kaolin in the CGFB sample.

The hydration product will infiltrate the kaolin particles. During slurry condensation, the hydration products in the matrix crystallize, and the CGFB samples material have a certain strength through ionic bonds and intermolecular forces. Now, alkaline inclusions gradually form on the surface of the kaolin particles. With an increase in the curing time from 0 to 28 days, kaolin particles are gradually eroded by alkaline inclusions, resulting in chemical changes and development of the active state. Because of the different ion concentrations inside and outside the coating, ion penetration expands the coating. When the pressure of the coating reaches its limit, the active component reacts with the ions to form C-S-H and other products. The formula for secondary hydration of kaolin is as follows:

$$SiO_2 + m_1Ca(OH)_2 + xH2O \rightarrow m_1CaO{\cdot}SiO_2{\cdot}xH_2O \quad (3)$$

$$Al_2O_3 + m_2Ca(OH)_2 + yH2O \rightarrow m_2CaO{\cdot}Al_2O_3{\cdot}yH_2O \quad (4)$$

The test results show that the strength of CGFB samples decreases with an increase in kaolin content. When the amount of kaolin instead of cement is 10%, the contribution of secondary hydration of some active components in kaolin to CGFB strength is lower than that of normal hydration of cement, but kaolin has a certain filling effect. Therefore, in the study, the strength of CGFB samples with kaolin sample decreased, but there is no significant difference compared with those of CGFB samples without kaolin, which is approximately 0.7 MPa. When the amount of kaolin is greater than 10%, the activity of kaolin is lower than that of cement, which mainly plays the role of filling. The decrease in cement content directly leads to a decrease in the hydration products in CGFB samples, a decrease in the cohesive force, and a consequent decrease in CGFB strength.

Therefore, considering requirements of CGFB strength for coal mine production safety, this study recommends replacing 10% cement in CGFB samples by kaolin as the most suitable option among those tested. That is to say, when the kaolin content is 10%, it can play a similar role as cement in CGFB samples and meet the mine-filling strength requirements. This paper mainly discusses the influence of kaolin on mechanical properties and microstructure of CGFB; however, carrying out systematic research on the durability and engineering applications of CGFB samples with kaolin is also necessary.

5. Conclusions

(1) The stress–strain curves of the CGFB samples are essentially the same, and they all pass through initial compaction, elastic deformation, plastic yield, and post-peak strain softening stages. The uniaxial compressive strength, peak strain, and elastic modulus decrease with the kaolin content. The average uniaxial compressive strength, elastic modulus, and peak strain of CGFB samples with 10% amount of kaolin are 0.68, 192.37, and 0.0053 MPa, respectively, which are close to those of CGFB samples with no kaolin.

(2) The kaolin content affects the failure characteristics of CGFB samples, which show tensile failure accompanied by local shear failure, and the failure degree increases

with the kaolin content. The fluctuation of Ra value of CGFB samples increases, and the difference of its cumulative Ra value decreases with the kaolin content, which increases tensile cracks in CGFB samples. The porosity of the fracture surface shows a decreasing trend as a whole. The reason is that the hydration is the main factor of kaolin affects the strength of CGFB samples, and the activity of kaolin is lower than that of cement. With the increase of kaolin content, the hydration of cement decreases, so the UCS of CGFB samples decreases. However, kaolin also fills the internal pores of CGFB samples, which improves their integrity and reduces the corresponding porosity. In summary, the porosity of CGFB samples decreases with the increase of kaolin, and the UCS gradually decreases.

(3) When the amount of kaolin is 10%, the internal structure of the CGFB sample is more compact, and the number of pores is less. When it is more than 10%, with an increase in the kaolin content, the decrease in cement content per unit volume leads to a decrease in the number of AFt and C-S-H gel, the peak of the SiO_2 diffraction peak becomes stronger, the C-S-H diffraction peak becomes weaker, and the number of irregular particles increases. As the average uniaxial compressive strength, elastic modulus, and peak strain of CGFB samples with 10% amount of kaolin are close to those of CGFB samples with no kaolin, replacing 10% cement in CGFB samples by kaolin is the most suitable option recommended.

Author Contributions: Conceptualization, D.Y.; methodology, D.Y.; software, F.L.; validation, C.Z., F.W. and N.J.; data curation, Z.Z.; writing-original draft preparation, F.L.; writing-review and editing, F.L. and D.Y.; funding acquisition, D.Y. All authors have read and agreed to the published version of the manuscript.

Funding: This research was funded by the National Science Foundation of China, grant number 51904167 and 52074169; the Taishan Scholars Project; the Taishan Scholar Talent Team Support Plan for Advantaged and Unique Discipline Areas; the SDUST Research Fund; and the Open Research Fund for the Key Laboratory of Safety and High-efficiency Coal Mining, grant number JYBSYS2019201.

Data Availability Statement: The data are available and explained in this article; readers can access the data supporting the conclusions of this study.

Conflicts of Interest: The authors declare no conflict of interest.

References

1. Miao, X.X.; Ju, F.; Huang, Y.L.; Guo, G.L. New progress and prospect of backfill mining theory and technology. *J. China Univ. Min. Technol.* **2015**, *44*, 391–399, 429.
2. Liu, Y.; Guo, Y.L.; Li, H.; Wang, H.Y. Experimental study on the influence of construction waste recycled aggregate on the transportation performance of mine CGFB. *J. Shandong Univ. Sci. Technol. Nat. Sci. Ed.* **2020**, *39*, 59–65.
3. Sun, X.K. Development status and prospect of green filling mining in mines. *Coal Sci. Technol.* **2020**, *48*, 48–55.
4. Liu, J.G.; Li, X.W.; He, T. Application status and development of filling mining in China. *J. China Coal Soc.* **2020**, *45*, 141–150.
5. Mo, Z.Y.; Liu, Y.L.; Wang, D.G.; Li, Z.J.; Bai, L.G. Research progress on mechanical properties of metakaolin cement based materials. *Chin. Ceram. Soc.* **2018**, *37*, 911–917.
6. Cao, Y.D.; Li, Y.X.; Zhang, J.S.; Cao, Z.; Sun, C.B. Effects of fineness and calcination temperature on pozzolanic activity and microstructure of coal gangue. *Chin. Ceram. Soc.* **2017**, *45*, 117–122.
7. Cheng, H.L.; Yang, F.H.; Ma, B.G.; Zhang, J.; Hao, L.W.; Liu, G.Q. Composite activation of high alumina gangue and analysis of its pozzolanic effect. *J. Build. Mater.* **2016**, *19*, 248–254.
8. Lin, C.; Li, J.X.; Chen, P.X.; Chen, G. Study on the influence of metakaolin on the compressive strength of concrete. *Guangdong Arch. Civ. Eng.* **2019**, *26*, 70–72.
9. Hou, L.Y.; Yang, A.R. Study on the influence of mineral admixtures on cement hydration properties. *Water Res. Hydropower Eng.* **2020**, *51*, 198–204.
10. Pang, J.Y.; Chen, X.P. Mechanical properties test of concrete with high active mineral admixture. *Chin. Ceram. Soc.* **2020**, *39*, 3143–3151.
11. Xi, Y.S. Effect of metakaolin admixture on workability and early mechanical properties of cement mortar. *China Concr.* **2019**, *8*, 72–76.
12. Jiang, G.; Rong, Z.D.; Sun, W. Effect of metakaolin on properties of high performance cement mortar. *J. Southeast Univ. Nat. Sci. Ed.* **2015**, *45*, 121–125.
13. Li, F.H.; Zhang, G.B.; Zhou, H.Y.; Zhou, S.; Li, G.H. Inhibitory effect of high activity metakaolin and fly ash on alkali aggregate reaction. *J. Build. Mater.* **2017**, *20*, 876–880.
14. Dong, M.; Ma, J.D.; Li, Y.F. Effect of metakaolin admixture on strength of cement mortar. *J. Mater. Sci. Eng.* **2020**, *38*, 295–300.

15. Liu, Y.Y. Application and Theoretical Study of Coal Series Kaolin Activation and Cement Admixture. Ph.D. Thesis, Wuhan University of Technology, Wuhan, China, 2018.
16. Wang, H. Process Mineralogy and Beneficiation Test of Sandy Kaolin. Master's Thesis, Wuhan University of Technology, Wuhan, China, 2013.
17. Yu, W. Mechanism of Metakaolin on Hydration Products of Cement Paste. Master's Thesis, Wuhan University of Technology, Wuhan, China, 2013.
18. Ebenezer, A.; Emmanuel, N.; Benjamin, A.T.; Stephen, K.A.; George, N.B.; Joanna, A.M.H.; Michael, O.P. Synthesis and Characterization of Modified Kaolin-Bentonite Composites for Enhanced Fluoride Removal from Drinking Water. *Adv. Mater. Sci. Eng.* **2021**, *2021*, 6679422.
19. Chen, M.N.; Chen, X.L.; Zhang, C.Y.; Cui, B.Z.; Li, Z.W.; Zhao, D.Y.; Wang, Z. Kaolin-Enhanced Superabsorbent Composites: Synthesis, Characterization and Swelling Behaviors. *Polymers* **2021**, *13*, 1204. [CrossRef]
20. Partha, D.; Tadikonda, V.B. Kaolin based protective barrier in municipal landfills against adverse chemo-mechanical loadings. *Sci. Rep.* **2021**, *11*, 1–12.
21. Chen, M.C.; Fang, W.; Xu, K.C. Effect of ceramic admixtures on performance of cement mortar. *Chin. Ceram. Soc.* **2015**, *34*, 793–798.
22. Wang, Z.Y.; Yao, S.Y. Structure and properties of animal bone ash doped Na_2O-CaO-SiO_2 Wollastonite Glass ceramics. *J. Shandong Univ. Sci. Technol. Nat. Sci. Ed.* **2020**, *39*, 48–55.
23. Zhang, H.W.; Elsworth, D.; Wan, Z.J. Failure response of composite rock-coal samples. *Geomech. Geophys. Geo-Energy Geo-Resour.* **2018**, *4*, 175–192. [CrossRef]
24. Yin, D.W.; Chen, S.J.; Liu, X.Q.; Ma, H.F. Effect of joint angle in coal on failure mechanical behavior of roof rock-coal combined body. *Q. J. Eng. Geol. Hydrogeol.* **2018**, *51*, 202–209. [CrossRef]
25. Yin, D.W.; Chen, S.J.; Chen, B.; Liu, X.Q.; Ma, H. Strength and failure characteristics of the rock-coal combined body with single joint in coal. *Geomech. Eng.* **2018**, *15*, 1113–1124.
26. Lu, Y.W.; Sun, C.P.; Shen, B.T. Experimental study on damage evolution and crack propagation characteristics of sandstone under combined stress. *J. Shandong Univ. Sci. Technol. Nat. Sci. Ed.* **2020**, *39*, 37–45.
27. Wang, Q.; Jiang, Z.H.; Jiang, B.; Gao, H.K.; Huang, Y.B.; Zhang, P. Research on an automatic roadway formation method in deep mining areas by roof cutting with high-strength bolt-grouting. *Int. J. Rock Mech. Min.* **2020**, *128*, 104264. [CrossRef]
28. Yin, S.J.; Chen, S.J.; Ge, Y.; Liu, R. Mechanical properties of rock–coal bi-material samples with different lithologies under uniaxial loading. *J. Mater. Res. Technol.* **2021**, *10*, 322–338. [CrossRef]
29. ASTM E569/E569M-13. *Standard Practice for Acoustic Emission Monitoring of Structures during Controlled Stimulation*; ASTM International: West Conshohocken, PA, USA, 2013; Available online: www.astm.org (accessed on 10 March 2021).
30. Sukpyo, K.; Hyeju, K.; Byoungky, L. Hydration Properties of Cement with Liquefied Red Mud Neutralized by Nitric Acid. *Materials* **2021**, *14*, 2641. [CrossRef]
31. Geuntae, H.; Sangwoo, O.; Seongcheol, C.; Won-Jong, C.; Young-Jin, K.; Chiwon, S. Correlation between the Compressive Strength and Ultrasonic Pulse Velocity of Cement Mortars Blended with Silica Fume: An Analysis of Microstructure and Hydration Kinetics. *Materials* **2021**, *14*, 2476. [CrossRef]
32. Cao, K.; Wang, L.; Xu, Y.; Shen, W.F.; Wang, H. The Hydration and Compressive Strength of Cement Mortar Prepared by Calcium Acetate Solution. *Adv. Civ. Eng.* **2021**, *2021*, 8817725. [CrossRef]
33. Tragazikis, I.K.; Kordatou, T.Z.; Exarchos, D.A.; Dalla, P.T.; Matikas, T.E. Monitoring the Hydration Process in Carbon Nanotube Reinforced Cement-Based Composites Using Nonlinear Elastic Waves. *Appl. Sci.* **2021**, *11*, 1720. [CrossRef]
34. Zhang, J.; Ke, G.J.; Liu, Y.Z. Early Hydration Heat of Calcium Sulfoaluminate Cement with Influences of Supplementary Cementitious Materials and Water to Binder Ratio. *Materials* **2021**, *14*, 642. [CrossRef]
35. Shiotani, T.; Ohtsu, M.; Ikeda, K. Detection and evaluation of AE waves due to rock deformation. *Constr. Build. Mater.* **2001**, *15*, 235–246. [CrossRef]
36. Liu, C.; Shi, B.; Zhou, J.; Tang, C. Qunication and characteriation of microporosity by image processing, geometric measurement and statistical methods: Application on SEM images of clay materials. *Appl. Clay Sci.* **2011**, *54*, 97–106. [CrossRef]
37. Liu, C.; Tang, C.; Shi, B.; Suo, W. Automatic quantification of crack patterns by image processing. *Comput. Geosci.* **2013**, *57*, 77–80. [CrossRef]
38. Liu, C.; Xu, Q.; Shi, B.; Gu, Y.F. Digital image recognition method of rock particle and pore system and its application. *Geotech. Eng.* **2018**, *40*, 925–931.
39. Urfels, S.; Bauer, J.; Vogel, H. General method of specimen preparation for the quantitative microscopic characterization of nano- and microparticles. *Mater. Charact.* **2019**, *153*, 60–68. [CrossRef]
40. Farnama, Y.; Geikerb, M.R.; Bentzc, D.; Weiss, J. Acoustic emission waveform characterization of crack origin and mode in fractured and ASR damaged concrete. *Cem. Concr. Compos.* **2015**, *60*, 135–145. [CrossRef]
41. Zingg, L.; Briffaut, M.; Baroth, J.; Malecot, Y. Influence of cement matrix porosity on the triaxial behaviour of concrete. *Cem. Concr. Res.* **2016**, *80*, 52–59. [CrossRef]
42. Chen, G.; Xu, P.; Mi, G.; Zhu, J. Compressive strength and cracking of composite concrete in hot-humid environments based on microscopic quantitative analysis. *Constr. Build. Mater.* **2019**, *225*, 441–451. [CrossRef]

43. Chen, J.L.; Zhang, N.; Li, H.; Zhao, X.B.; Liu, X.M. Study on hydration characteristics of red mud based paste like filling materials. *Chin. J. Chem. Eng.* **2017**, *39*, 1640–1646.
44. Li, Y.C.; Min, X.B.; Ke, Y.; Chai, L.Y.; Shi, M.Q.; Tang, C.J.; Wang, Q.W.; Liang, Y.J.; Lei, J.; Liu, D.G. Utilization of red mud and Pb/Zn smelter waste for the synthesis of a red mud-based cementitious material. *J. Hazard. Mater.* **2018**, *344*, 343–349. [CrossRef] [PubMed]
45. Andini, S.; Cioffi, R.; Colangelo, F. Coal fly ash as raw material for the manufacture of geopolymer-based products. *Waste Manag.* **2008**, *28*, 416–423. [CrossRef] [PubMed]
46. Singh, M.; Upadhayay, S.N.; Prasad, P.M. Preparation of iron rich cements using red mud. *Cem. Concr. Res.* **1997**, *27*, 1037–1046. [CrossRef]